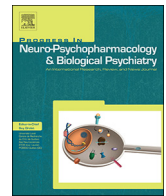




Contents lists available at ScienceDirect

# Progress in Neuropsychopharmacology & Biological Psychiatry

journal homepage: [www.elsevier.com/locate/pnp](http://www.elsevier.com/locate/pnp)

## Riemannian classifier enhances the accuracy of machine-learning-based diagnosis of PTSD using resting EEG

Yong-Wook Kim<sup>a,b</sup>, Sungkean Kim<sup>a,b</sup>, Miseon Shim<sup>c</sup>, Min Jin Jin<sup>b,d</sup>, Hyeonjin Jeon<sup>b</sup>,  
Seung-Hwan Lee<sup>b,e,\*</sup>, Chang-Hwan Im<sup>a,\*\*</sup>

<sup>a</sup> Department of Biomedical Engineering, Hanyang University, Seoul, Republic of Korea

<sup>b</sup> Clinical Emotion and Cognition Research Laboratory, Inje University, Goyang, Republic of Korea

<sup>c</sup> Department of Psychiatry, University of Missouri-Kansas City, Kansas City, MO, USA

<sup>d</sup> Department of psychology, Chung-Ang University, Seoul, Republic of Korea

<sup>e</sup> Department of Psychiatry, Inje University, Ilsan-Paik Hospital, Goyang, Republic of Korea

### ARTICLE INFO

#### Keywords:

Post-traumatic stress disorder  
Machine learning  
Computer-aided diagnosis  
Classification  
Riemannian geometry

### ABSTRACT

Recently, objective and automated methods for the diagnosis of post-traumatic stress disorder (PTSD) have attracted increasing attention. However, previous studies on machine-learning-based diagnosis of PTSD with resting-state electroencephalogram (EEG) have reported poor accuracies of as low as 60%. Here, a Riemannian geometry-based classifier, the Fisher geodesic minimum distance to the mean (FgMDM), was employed for PTSD classification for the first time. Eyes-closed resting-state EEG data of 39 healthy individuals and 42 PTSD patients were used for the analysis. EEG source activities in 148 cortical regions were parcellated based on the Destrieux atlas, and their covariances were evaluated for each individual. Thirty epochs of preprocessed EEG were employed to calculate source activities. In addition, the FgMDM approach was applied to each EEG source covariance to construct the classifier. For a comparison, linear discriminant analysis (LDA), support vector machine (SVM), and random forest (RF) classifiers employing source band powers and network features as feature candidates were also tested. The FgMDM classifier showed an average classification accuracy of 75.240.80%. In contrast, the maximum accuracies of LDA, SVM, and RF classifiers were  $66.54 \pm 2.99\%$ ,  $61.11 \pm 2.98\%$ , and  $60.99 \pm 2.19\%$ , respectively. Our study demonstrated that the diagnostic accuracy of PTSD with resting-state EEG could be significantly improved by employing the FgMDM framework, which is a type of Riemannian geometry-based classifier.

### 1. Introduction

Post-traumatic stress disorder (PTSD) is a mental disorder in which dysfunctional brain activities are observed after a traumatic event. The typical symptoms of PTSD as defined by the Diagnostic and Statistical Manual of Mental disorders (DSM-V) include re-experiencing, avoidance/numbing, and hyperarousal (Friedman et al., 2011). A large proportion of individuals (60% of men and 50% of women) are exposed to traumatic events more than once in their whole lifespan (Lobo et al., 2015), and the lifetime prevalence of PTSD for the general population is

reported to be approximately 6.8% in the USA (Kessler et al., 2005). To date, PTSD diagnosis is performed mostly based on self reports (Friedman, 2015; Lobo et al., 2015; Meyer et al., 2018); however, with the recent development of neuroimaging methods, unbiased, objective, and automated methods for the diagnosis of PTSD have attracted increasing attention (Christova et al., 2015; Liu et al., 2015). These automated diagnosis methods can not only provide a useful option for early detection of chronic PTSD (Galatzer-Levy et al., 2014) but also deliver a unique method to diagnose PTSD in infants or young children from whom reliable self-reports can rarely be obtained (Scheeringa

**Abbreviations:** AUC, Area under the curve; BCI, Brain-computer interface; BE, Boundary element; CAPS, Clinician-Administered PTSD scale; DSM-V, Diagnostic and Statistical Manual of Mental disorders; ERP, Event related potential; FFT, Fast Fourier transform; FgMDM, Fisher geodesic minimum distance to the mean; HC, Healthy controls; LDA, Linear discriminant analysis; PCA, Principal component analysis; PET, Positron emission tomography; PSD, Power spectral density; PTSD, Post-traumatic stress disorder; RF, Random forest; SCM, spatial covariance matrix; SVM, Support vector machine; qEEG, quantitative electroencephalogram

\* Correspondence to: S.-H. Lee, Department of Psychiatry, Ilsan Paik Hospital, Inje University College of Medicine, Juhwa-ro 170, Ilsanseo-Gu, Goyang 10380, Republic of Korea.

\*\* Correspondence to: C.-H. Im, Department of Biomedical Engineering, Hanyang University, 222 Wangsimni-ro, Seongdong-gu, Seoul 04763, Republic of Korea.

E-mail addresses: [lshpss@paik.ac.kr](mailto:lshpss@paik.ac.kr) (S.-H. Lee), [ich@hanyang.ac.kr](mailto:ich@hanyang.ac.kr) (C.-H. Im).

<https://doi.org/10.1016/j.pnpbp.2020.109960>

Received 22 November 2019; Received in revised form 19 April 2020; Accepted 30 April 2020

Available online 03 May 2020

0278-5846/ © 2020 Published by Elsevier Inc.

et al., 1995).

Electroencephalogram (EEG) is one of the most viable options to implement the computer-aided diagnosis of PTSD because EEG has proven to provide reliable biomarkers of brain dysfunction (Fingelkurts and Fingelkurts, 2015). EEG also has several advantages over other neuroimaging modalities such as functional magnetic resonance imaging (fMRI) and positron emission tomography (PET) in that it exhibits a high temporal resolution, is economical, and can be made portable (Coburn et al., 2006; Lobo et al., 2015). Some previous studies have reported close relationships between the features of EEG and PTSD. The relationships were observed in event related potentials (ERPs) (Covey et al., 2013; Karl et al., 2006; Lobo et al., 2014; Metzger et al., 2008), quantitative EEG (qEEG) band powers especially in alpha (Imperatori et al., 2014; Sheerin et al., 2018; Wahbeh and Oken, 2013), and alpha asymmetry (Kemp et al., 2010; Rabe et al., 2006).

Although several potential EEG biomarker candidates for PTSD diagnosis have been reported, only one study succeeded in classifying PTSD patients and healthy controls (HCs) with an accuracy over 70%. Attias et al. (1996) argued that PTSD patients and HCs could be classified with fairly high accuracies of 95% and 85%, respectively, by employing P3 peak amplitudes and P3 latencies as features for Fisher's linear discriminant analysis (LDA). However, this result is very controversial because data of only four representative subjects out of 20 in each group were used to train the LDA classifier and no cross validation was performed. Indeed, Falconer et al. (2008) reported that they classified PTSD and HC with an accuracy of 77.3% by employing P3 and other physiological and cognitive measures as features; however, P3 features were never included in the top four predictors. Based on this relatively more recent study, the diagnostic accuracy reported by Attias et al. (1996) might be overestimated. On the other hand, machine-learning-based classification of PTSD and HC with resting-state EEG is generally more practical than that with ERPs such as P3 because resting-state EEG can be recorded more easily than ERPs without the requirement of repeated task trials. Indeed, resting-state EEG can be recorded in a short period of time with economical portable EEG devices (Casson, 2019; Park and Choi, 2019). However, Rozgic et al. (2014) and Zhuang et al. (2014), who employed EEG spectral powers as the features for the machine learning, reported low maximum area under curve (AUC) of 0.62 and F-measures of 0.62, respectively. Therefore, the performance of classifying PTSD and HC with resting-state EEG needs to be further improved.

Recently, classification of EEG based on Riemannian geometry has been actively studied (Congedo et al., 2017). A number of articles regarding diverse research topics, such as motor imagery BCI (Barachant et al., 2011; Han et al., 2019; Barachant et al., 2013a, 2013b), sleep stage classification (Li et al., 2012), mental fatigue detection (Roy et al., 2014), auditory and tactile P300 BCI (Rutkowski et al., 2018), and seizure detection (Yuan et al., 2016), have reported excellent performance of Riemannian geometry-based classifiers compared to Euclidean space-based traditional classifiers. Riemannian geometry-based classifiers have also been successfully applied to diagnostic classification of neuropsychiatric diseases. Gemein et al. (2020) classified HC and patients with Alzheimer's disease, strokes, depression, or epilepsy by applying Riemannian geometry-based classifiers with an average accuracy of 85.87%. Sadatnejad et al. (2019) developed Riemannian-based SVM by employing multiple instance learning, and classified attention deficit hyperactivity disorder vs. bipolar mood disorder, schizophrenia vs. HC, and depression vs. HC, with fairly high classification accuracies. Based on the above articles, it was expected that the performance of classifying PTSD and HC with resting-state EEG might be improved by employing Riemannian geometry-based classifiers.

In this study, we investigated whether a classifier based on Riemannian geometry can increase the accuracy of classifying PTSD and HC. Even though recent studies have demonstrated that Riemannian geometry-based classifiers could be successfully applied to various EEG classification problems (Congedo et al., 2017; Barachant

et al., 2010; Barachant et al., 2013a, 2013b), they have never been applied to the classification of PTSD and HC with resting-state EEG. We employed the Fisher geodesic minimum distance to the mean (FgMDM) classifier as the Riemannian geometry-based classifier (Barachant et al., 2010; Davoudi et al., 2017). To compare the classification performance of the FgMDM classifier and various conventional classifiers, LDA, support vector machine (SVM), and random forest (RF) classifiers employing source band powers and network measures as features were also evaluated. The best classification results achieved by FgMDM and the conventional classifiers were quantitatively compared to demonstrate that the Riemannian geometry-based classifiers could yield better performance than that of the conventional classifiers.

## 2. Methods

### 2.1. Participants

Forty-two patients with PTSD (5 men and 37 women; age:  $40.12 \pm 11.07$ ) and thirty-nine HCs (8 men and 31 women; age:  $41.15 \pm 12.31$ ) participated in this study. PTSD patients were diagnosed using the Structured Clinical Interview for DSM-V (SCID) Axis I Psychiatric Disorders (American Psychiatric Association, 2013) by an experienced psychiatrist. Clinician-Administered PTSD scale (CAPS) (Blake et al., 1995) and PTSD checklist (PCL) (Weathers et al., 1993) were used to evaluate psychiatric symptoms. HCs were recruited from the local community through flyers, posters, or newspapers. Only individuals without mild traumatic brain injury, organic brain disorder, and mood/anxiety disorder were allowed to participate in this study. Participants who were older than 55 years, smokers, and those who had a lifetime history of alcohol or drug abuse were excluded from this study. All participants signed a written informed consent form approved by the Institutional Review Board of Inje University, Ilsan Paik Hospital (IRB no. 2015-07-025). The demographic data of the participants are reported in Table 1. The independent *t*-test was employed to compare the age, education years, CAPS, and PCL scores, and the chi-square test was employed to compare the sex ratio.

### 2.2. EEG recording and pre-processing

All EEG data were recorded while the participants were in the relaxed state with their eyes closed for 3 min. The participants were asked to sit on a chair in a slightly dim room and asked not to move or sleep during the EEG recording. EEG signals were recorded using a NeuroScan SynAmps amplifier (Compumedics USA, Charlotte, NC, USA) with 62 Ag/AgCl electrodes mounted on NeuroScan Quik-Cap according to the extended international 10-20 system. The sampling rate was set at 1000 Hz, and the recorded EEG data were filtered using a 0.1-100 Hz bandpass filter. The impedances of all electrodes were adjusted not to exceed 5 k $\Omega$ . The ground electrode was placed on the forehead, and the reference electrode was placed above Cz.

**Table 1**

Demographic characteristics of all study participants. The numbers in the parentheses in the "sex" were the percentage of male or female in each group.

	PTSD patients (N = 42)	Healthy controls (N = 39)	<i>p</i>
Age (years)	40.12 $\pm$ 11.07	41.15 $\pm$ 12.31	0.691
Sex			0.302
Male	5 (11.9)	8 (20.5)	
Female	37 (88.1)	31 (79.5)	
Education (years)	12.67 $\pm$ 3.73	14.21 $\pm$ 3.11	0.048
CAPS	50.45 $\pm$ 13.72	7.31 $\pm$ 9.26	< 0.001
PCL	46.83 $\pm$ 16.53	11.62 $\pm$ 10.31	< 0.001

CAPS: Clinician-Administered PTSD scale; PCL: Post-traumatic Stress Disorder Checklist.

Raw EEG data were preprocessed using CURRY 7 software (Compumedics USA, Charlotte, NC, USA) and MATLAB R2016b (MathWorks, Natick, MA, USA). After re-referencing with the common average reference, baseline correction was performed by removing each channel's DC offset from the EEG data. Gross artifacts such as movement artifacts were rejected by a trained researcher without any prior information regarding the data. Eye movement or eye blink artifacts were removed using the mathematical procedure implemented in CURRY 7 (Semlitsch et al., 1986). The EEG data were then filtered by employing a third order Butterworth IIR bandpass filter with forward-backward zero phase filtering process with cutoff frequencies of 1 and 50 Hz. Whole EEG data were divided by several 2 s epochs, and epochs containing significantly large physiological artifacts (amplitude  $> \pm 75 \mu\text{V}$ ) were excluded from the analysis. For each epoch, powers of theta band (4–8 Hz) and alpha band (8–12 Hz) were calculated using fast Fourier transform (FFT). Then, the theta/alpha ratio was calculated and averaged across 62 electrodes for each epoch. Any epoch in which the theta/alpha ratio exceeded 1 was rejected because it was thought that the participant felt drowsy or fell in sleep stage I when the theta power exceeded alpha power (Šušmáková and Krakovská, 2007; Hsu et al., 2013; Bareham et al., 2015). Note that theta power showed positive correlation with sleepiness and alpha power showed negative correlation with sleepiness (Strijkstra et al., 2003). Finally, thirty epochs were randomly selected from the remaining epochs and used for further analyses.

### 2.3. Source localization

To estimate cortical source activities, a depth-weighted minimum L2 norm estimator implemented in the brainstorm toolbox was used (Tadel et al., 2011). A three-layer boundary element (BE) model was constructed from the Colin27 standard brain template using the OpenMEEG project software (Gramfort et al., 2010), and a leadfield matrix was constructed with this BE model. The cortical current density values at 15,002 cortical vertices were evaluated at every timepoint in each epoch without a source orientation constraint. Noise covariance was evaluated using whole epochs of each person. Only diagonal components of noise covariance were used to calculate the weight of each individual sensor. EEG source time-series in each of the 148 cortical regions were parcellated based on the Destrieux atlas and then extracted by applying principal component analysis (PCA) to the time-series of all vertices included in each of the parcellated cortical regions.

### 2.4. Classification

A Riemannian geometry-based classifier as well as LDA, SVM, and RF classifiers were used to classify PTSD and HC groups. The Riemannian geometry-based classifier uses source covariance matrices as features to classify each group (Barachant et al., 2010). This framework first extracts spatial covariance matrices (SCMs) for each class. In this study, the size of each SCM was  $148 \times 148$  because we employed 148 brain regions. The Riemannian average matrices were computed using SCMs for each class and mapped onto the Riemannian tangent space. Through this mapping process, called tangent space mapping, the matrices can be vectorized and dealt with like Euclidean objects. Tangent space mapping allows the use of advanced classifiers that were available only in Euclidean space within the Riemannian space (Congedo et al., 2017). In this study, FgMDM was selected as the classifier, which was composed of the minimum distance to the mean (MDM) method and the geodesic filter (Barachant et al., 2010; Davoudi et al., 2017). The MDM method classifies each class by comparing the distance between covariance of each subject and average covariance of each class. The Riemannian mean and Riemannian distance were used for the MDM method (Barachant et al., 2011). The geodesic filter was employed to discard irrelevant information (noise) that might affect the distance. Before applying the FgMDM classifier, the entire frequency

band (4–50 Hz) was divided into five sub-bands: theta ( $\theta$ : 4–8 Hz), alpha ( $\alpha$ : 8–12 Hz), low beta ( $\beta_1$ : 12–18 Hz), late beta ( $\beta_2$ : 18–30 Hz), and gamma ( $\gamma$ : 30–50 Hz). Then, fifteen frequency bands were formed by successively merging neighboring frequency bands ( $\theta / \alpha / \beta_1 / \beta_2 / \gamma / \theta + \alpha / \alpha + \beta_1 / \beta_1 + \beta_2 / \beta_2 + \gamma / \theta + \alpha + \beta_1 / \alpha + \beta_1 + \beta_2 / \beta_1 + \beta_2 + \gamma / \theta + \alpha + \beta_1 + \beta_2 / \alpha + \beta_1 + \beta_2 + \gamma / \theta + \alpha + \beta_1 + \beta_2 + \gamma$ ). The source time-series corresponding to each of the 15 frequency bands was found by applying a bandpass filter. SCMs were then evaluated using the filtered source activities for each of the 15 frequency bands. A 10-fold cross-validation was performed repeatedly 10 times to calculate the average classification accuracy, sensitivity, specificity, and AUC. In each cross-validation, each participant's 30 SCMs, each corresponding to each epoch, were tested and the class into which more SCMs were classified was determined as the class of the participant. The AUC of FgMDM were calculated based on the methods in the Barachant and Congedo (2014). The accuracy, sensitivity, specificity, and AUC values were averaged within each 10-fold cross-validation, and averaged across the 10 repeated runs. The Covariance Toolbox was used for these analyses (<https://github.com/alexandrebarachant/covariantoolbox>). The source code for this analysis is available at Figshare (<https://figshare.com/s/a8e72f2c1202931b7779>).

Source band powers and their global/nodal network measures were used as the features of the traditional classifiers (LDA, SVM, and RF). The network measures were employed to compensate for the information of connectivity among the cortical regions, which was inherently considered in the covariance matrix used in the FgMDM. The global network measures were clustering coefficient, path length, global efficiency, and global strength (Rubinov and Sporns, 2010). The nodal network measures were nodal clustering coefficient and eigenvector centrality (Rubinov and Sporns, 2010; Ruhnau, 2000). The frequency bands were separated into eleven sub-frequency bands: theta (4–8 Hz), alpha (8–12 Hz), beta (12–30 Hz), gamma (30–50 Hz), low alpha (8–10 Hz), high alpha (10–12 Hz), low beta (12–18 Hz), mid beta (18–22 Hz), high beta (22–30 Hz), early beta (12–22 Hz), and late beta (18–30 Hz). We divided the frequency bands more specifically to improve the overall classification performance by generating more numbers of feature candidates. To extract the source power spectral density (PSD) features, FFT was applied to source time-series of each of the 148 regions. The average spectral power of each cortical region at each frequency band was calculated by averaging the spectral powers of the 30 selected epochs. Consequently, 1628 spectral power features ( $148 \text{ regions} \times 11 \text{ frequency bands}$ ), 44 global network measures ( $4 \text{ network measures} \times 11 \text{ frequency bands}$ ), and 3256 nodal network measures ( $2 \text{ network measures} \times 148 \text{ regions} \times 11 \text{ frequency bands}$ ) were evaluated for each trial. Each of the three different feature types was independently employed for the classification, and all features (4928 features in total) were also used for the classification. A 10-fold cross-validation was performed 10 times to calculate the average classification accuracy. For each cross validation, Fisher scores were evaluated to select the best feature subset for the current training dataset, and only 1 to 20 features with the highest Fisher scores were selected to prevent potential over-fitting of the data (Shim et al., 2016). Classification was performed with LDA, SVM with radial kernel basis function, and RF classifiers (Breiman, 2001; Duda et al., 2012; Scholkopf et al., 1997). The accuracies, sensitivities, specificities, and AUCs were averaged in 10-fold cross-validation and averaged across the 10 times runs. The average accuracy, sensitivity, specificity, and AUC were calculated per 1 to 20 selected features. A MATLAB toolbox, prtools 5.3.3 (<http://37steps.com>), was used for these analyses.

## 3. Results

The accuracy, sensitivity, specificity, and AUC obtained from FgMDM, LDA, SVM, and RF methods are shown in Table 2. Only the maximum accuracy for the LDA, SVM, and RF methods was presented

**Table 2**  
The average classification accuracy of FgMDM classifier and the maximum accuracies of the conventional classifiers.

Classifiers	Feature <sup>a</sup>		Accuracy (%)	Sensitivity (%)	Specificity (%)	AUC
FgMDM	Source covariance	(1)	73.09 ± 2.08	68.72 ± 3.78	77.14 ± 2.30	0.7970 ± 0.0141
LDA	All	(3)	63.95 ± 3.33	71.67 ± 4.69	55.64 ± 3.43	0.5357 ± 0.0297
	Source band power	(3)	66.42 ± 2.65	73.57 ± 3.06	58.72 ± 3.30	0.5534 ± 0.0456
SVM	Global network	(1)	54.69 ± 1.93	66.90 ± 2.08	41.54 ± 2.91	0.4969 ± 0.0279
	Local network	(6)	58.02 ± 3.19	65.24 ± 4.38	50.26 ± 4.22	0.5045 ± 0.0300
	All	(2)	64.57 ± 2.26	75.00 ± 3.02	53.33 ± 4.32	0.6432 ± 0.0613
	Source band power	(3)	62.35 ± 4.21	63.81 ± 5.81	60.77 ± 4.99	0.6252 ± 0.0459
	Global network	(16)	51.73 ± 3.05	80.48 ± 3.86	20.77 ± 5.60	0.4634 ± 0.0672
	Local network	(18)	52.22 ± 0.83	98.33 ± 1.15	2.56 ± 1.71	0.5950 ± 0.0433
RF	All	(11)	61.98 ± 3.63	67.86 ± 3.41	55.64 ± 5.41	0.6635 ± 0.0659
	Source band power	(14)	60.74 ± 2.31	67.86 ± 4.38	53.08 ± 5.80	0.6310 ± 0.0497
	Global network	(20)	54.20 ± 4.49	58.81 ± 5.94	49.23 ± 4.49	0.5292 ± 0.0613
	Local network	(4)	54.44 ± 3.79	59.76 ± 5.08	48.72 ± 5.27	0.5355 ± 0.0609

FgMDM: Fisher geodesic minimum distance to the mean; LDA: Linear discriminant analysis; SVM: Support vector machine; RF: Random forest.

<sup>a</sup> The numbers in the parentheses represent the number of features when the maximum accuracy was achieved.

among the 20 classification results corresponding to 1 to 20 features, and the sensitivity, specificity, and AUC yielding the maximum classification accuracy were presented. The FgMDM classifier outperformed other conventional classifiers in terms of the average classification accuracy. The average classification accuracy of the FgMDM classifier with full-band source covariance was reported to be 73.09 ± 2.08%. The minimum and maximum accuracies were 69.14% and 76.54%, respectively. The average sensitivity and specificity were 68.72 ± 3.78% and 77.14 ± 2.30%, respectively. The AUC was 0.7970 ± 0.0141. The conventional classifiers showed relatively lower classification accuracies. The maximum classification accuracy of LDA was 66.42 ± 2.65% when source band powers were used as features. The sensitivity was 73.57 ± 3.06%, and the specificity was 58.72 ± 3.30%. The AUC was 0.5534 ± 0.0456. The maximum classification accuracy of SVM was 64.57 ± 2.26% when all the features were used, and its sensitivity, specificity, and AUC were 75.00 ± 3.02%, 53.33 ± 4.32%, and 0.6432 ± 0.0613, respectively. The maximum classification accuracy of the RF method was 61.98 ± 3.63%, when source band powers were used as features. The sensitivity, the specificity, and AUC were 67.86 ± 3.41%, 55.64 ± 5.41%, and 0.6635 ± 0.0659 respectively.

Table 3 shows the frequency bands of the top ten FgMDM classifiers that yielded the highest classification accuracy. The maximum accuracy was reported to be 73.09 ± 2.08% when the whole band SCM was employed. The second highest accuracy was 72.72 ± 2.21% when the feature was 8–50 Hz band SCM, while the third highest accuracy was 72.59 ± 2.08% when the feature was 4–30 Hz band SCM. The accuracy tended to increase with increasing bandwidth.

#### 4. Discussion

In this study, we classified PTSD patients and HCs by applying a

**Table 3**  
The classification accuracies of the FgMDM classifier with respect to different frequency bands.

Band	Accuracy (%)	Sensitivity (%)	Specificity (%)	AUC
4–50 Hz	73.09 ± 2.08	68.72 ± 3.78	77.14 ± 2.30	0.7970 ± 0.0141
4–18 Hz	71.98 ± 3.86	66.67 ± 3.82	76.90 ± 4.63	0.7666 ± 0.0288
4–30 Hz	72.59 ± 2.08	67.69 ± 2.48	77.14 ± 3.01	0.7907 ± 0.0145
8–18 Hz	68.52 ± 2.75	62.82 ± 4.72	73.81 ± 3.17	0.7524 ± 0.0233
8–30 Hz	70.49 ± 2.36	64.10 ± 2.96	76.43 ± 2.37	0.7722 ± 0.0157
8–50 Hz	72.72 ± 2.21	66.67 ± 2.96	78.33 ± 2.62	0.7903 ± 0.0192
12–30 Hz	71.23 ± 1.93	66.92 ± 3.51	75.24 ± 2.01	0.7578 ± 0.0312
12–50 Hz	70.99 ± 2.12	63.59 ± 5.10	77.86 ± 1.15	0.7743 ± 0.0099
18–30 Hz	70.00 ± 5.04	67.95 ± 8.13	71.90 ± 4.17	0.7482 ± 0.0114
18–50 Hz	72.10 ± 2.92	66.41 ± 4.75	77.38 ± 2.31	0.7752 ± 0.0137
30–50 Hz	70.25 ± 2.36	64.62 ± 2.65	75.48 ± 3.18	0.7825 ± 0.0107

Riemannian geometry-based FgMDM classifier to resting-state qEEG data for the first time. The performance of the FgMDM classifier was compared with those of conventional classifiers—LDA, SVM, and RF—in terms of classification accuracy. The FgMDM classifier outperformed other conventional classifiers and exhibited the best average classification accuracy of 73.09% and the best AUC of 0.7970. The classification accuracies of the conventional classifiers (LDA, SVM, and RF) were about 7–12% lower than that of the FgMDM classifier. The maximum classification accuracies of LDA, SVM, and RF were reported to be 66.42%, 64.57%, and 61.98%, respectively.

There were only two articles that attempted to classify PTSD and HC by employing spectral powers as features (Rozgic et al., 2014; Zhuang et al., 2014). Rozgic et al. (2014) classified PTSD and HC by employing the EEG, ECG, GSR, motion, speech as features. They employed SVM as the classifier. When only EEG features were used, the AUC was 0.62. In our results, the best AUC of FgMDM was 0.7970, and the best AUC of LDA, SVM, and RF were 0.5031, 0.5366, and 0.4708, respectively. The FgMDM showed much larger AUC than that of Rozgic et al. (2014). Zhuang et al. (2014) classified PTSD and HC by employing speech, EEG, and its combination as features, and reported the performance in terms of F-measures. When only EEG features were used for SVM classification, the best reported F-measure was 0.62. In our results, the F-measure of FgMDM was 0.7109, and F-measures of LDA, SVM, RF were 0.6182, 0.6408, and 0.5933, respectively. The FgMDM showed the best F-measure value, whereas the F-measures of conventional classifiers were almost equal to the result of Zhuang et al. (2014).

Riemannian geometry-based classifiers have been reported to improve the classification accuracy in various EEG classification studies and have been found to outperform conventional classifiers in sleep stage detection (Li et al., 2009), motor imagery-based brain-computer interface (Barachant et al., 2011), steady-state visual evoked potential-based brain-computer interface (Kalunga et al., 2016). Riemannian

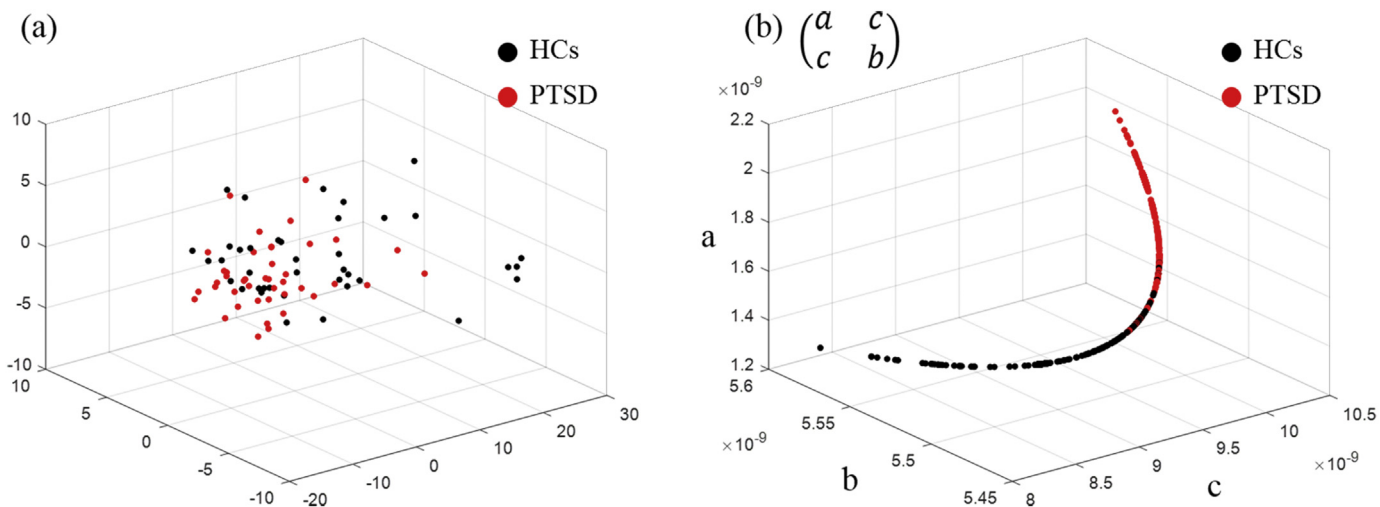


**Fig. 1.** Examples of feature vector distributions used for (a) conventional classifiers and (b) FgMDM method with an applied geodesic filter. Dimensionality of each figure was reduced using principal component analysis (Harandi et al., 2017) and the supervised dimensionality reduction method (Harandi et al., 2017; Rodrigues et al., 2017).

geometry-based classifiers are known to better reflect the complex and non-linear characteristics of EEG than the conventional classifiers. According to Horev et al. (2015), EEG signals could not be modeled just with simple Gaussian assumption as the generation of EEG signals involves complex and non-linear phenomena. Moreover, because the etiology of PTSD is known to be multi-causal, multi-modal, and complex (Galatzer-Levy et al., 2014), Riemannian geometry-based classifiers are more appropriate for classification of PTSD patients and HCs than conventional classifiers. Fig. 1 shows examples of feature distributions of the conventional methods and the FgMDM method.

Even though SCM features are used, the classification accuracy can depend on methods for evaluating the distance between each participant's SCM and the average SCMs of each class. We tested three different methods to calculate the distances—Euclidean distances, Riemannian distances on MDM without geodesic filter, and Riemannian distances that were calculated from geodesic filtered SCMs in FgMDM methods. On the abscissa of Fig. 2, the distances between each participant's SCM and the average SCM of PTSD patients are shown, whereas on the ordinate of Fig. 2, the distances between each participant's SCM and the average SCM of HC are shown. The distances from each class

could be clearly differentiated when the FgMDM classifier was employed (right). The distances could also be differentiated fairly well with the MDM without the geodesic filter (middle). However, when the same process was applied on Euclidean space, differentiating each class by solely using the distance value (left) was difficult. These results suggest that some information differentiating PTSD and HC might not be accessible on Euclidean distance but might be accessible on the Riemannian distance, as discussed by Barachant et al. (2011).

A geodesic filter might also be an important factor that can further increase the classification accuracy. Barachant et al. (2010) proposed Fisher geodesic discriminant analysis which is an extension of Fisher LDA applied to the tangent space. Employing a geodesic filter can be a solution to overcome the disadvantages of MDM; MDM performs poorly in high dimension (Congedo et al., 2019) and is known to be vulnerable to noise (Davoudi et al., 2017). Table 4(a) compares the performances of the MDM and FgMDM approaches, in terms of classification accuracy, and shows that the FgMDM approach outperformed the MDM approach.

Extracting source-level features instead of sensor-level features might also contribute to the enhancement of classification accuracy.

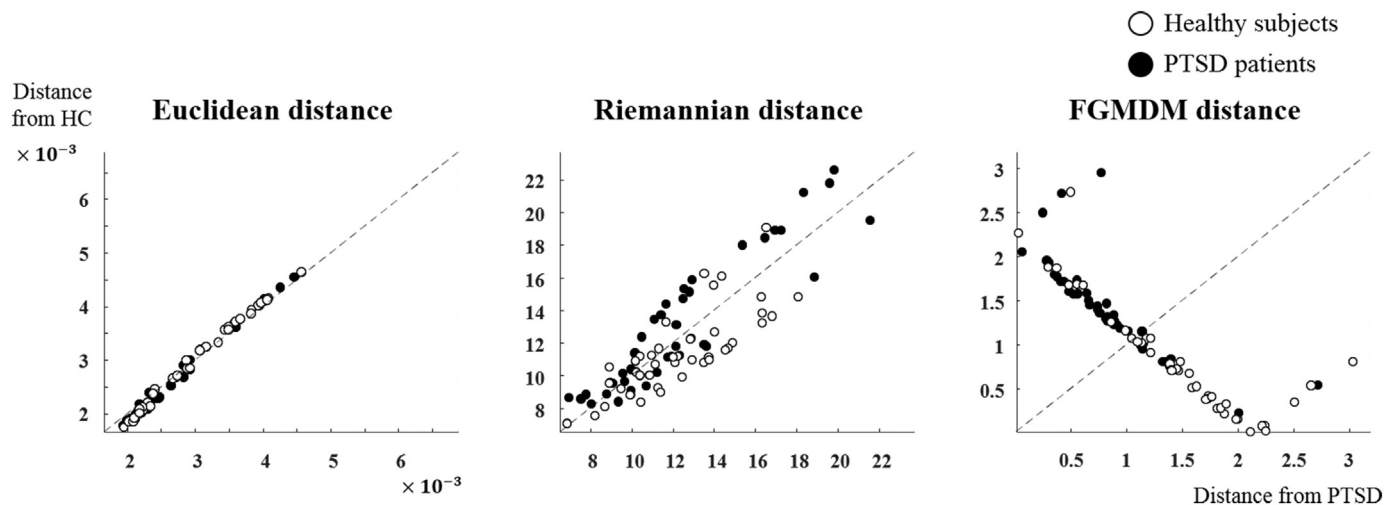


**Fig. 2.** Distances between each participant's SCM and the average SCM of each group evaluated using the three different methods (Euclidean distance, Riemannian distance (MDM), and FgMDM). The distances between SCM of each subject and the average SCM of PTSD patients are shown on the abscissa, whereas the distances between SCM of each subject and the average SCM of HC are shown on the ordinate. The dotted line indicates the cases when the distances from PTSD and HC group averages are the same.

**Table 4**

(a) The classification accuracies of MDM and FgMDM classifiers (source SCM was used), and (b) the classification accuracies of FgMDM classifiers built with sensor-level and source-level SCMs.

Classifiers	Accuracy (%)	Sensitivity (%)	Specificity (%)
FgMDM	73.09 ± 2.08	68.72 ± 3.78	77.14 ± 2.30
MDM	64.43 ± 1.12	68.48 ± 2.80	60.06 ± 3.38

SCMs	Accuracy (%)	Sensitivity (%)	Specificity (%)
Source-level	73.09 ± 2.08	68.72 ± 3.78	77.14 ± 2.30
Sensor-level	67.26 ± 1.90	64.50 ± 2.86	70.88 ± 3.23

One of the disadvantages of EEG is the low spatial resolution originating from the volume conduction effect. Poor signal to noise ratio due to artifacts and noises is also a disadvantage of EEG. EEG source imaging could be an alternative to circumvent these disadvantages. Various studies have reported increased classification performance by employing source-level EEG features, examples of which include the motor imagery-based brain-computer interface (BCI) (Ahn et al., 2012), ERP-based BCI (Goel et al., 2011), and EEG-based automatic diagnosis of schizophrenia (Shim et al., 2016). According to Ahn et al. (2012), some information could be visible only in the source space because source imaging enables filtering out some noise components. Table 4(b) shows the effect of using source-level features on the classification performance. The SCMs from the sensor-level EEG signals were computed based on the same method used for the computation of source-level SCMs. The size of each SCM was 62 × 62 as 62 electrodes were used for EEG recording. The performance of the FgMDM classifier with SCMs from EEG source activities was superior to that with SCMs from the sensor-level EEG signals, in terms of accuracy, sensitivity, and specificity.

Table 3 presents the changes of the classification performance with respect to the different frequency bands. The best performance was obtained when the whole frequency band was used. Indeed, many previous studies have reported that EEG recorded from patients with PTSD generally show abnormalities in almost all frequency bands. For example, in the theta band, increase of theta activity in the parietal lobes and decrease of theta band activity over temporal lobe, frontal lobes, and central lobe in PTSD patients were observed (Imperatori et al., 2014; Todder et al., 2012; Cowdin et al., 2014; Woodward et al., 2000). In alpha band, Imperatori et al. (2014) reported the increase of alpha band connectivity in PTSD patients, and Wahnhe et al., (2013) reported higher alpha frequency peak in PTSD. In beta band, PTSD patients showed increased beta band power in REM sleep stage (Woodward et al., 2000) and exhibited decrease of nodal degree and nodal efficiency in frontal and central regions (Lee et al., 2014). In gamma band, Lee et al. (2014) reported decrease of nodal degree and nodal efficiency in frontal and central lobe, and Ehlers et al. (2006) reported significant increase in frontal EEG gamma band activity in PTSD patients.

There are some limitations in our present study. First, the years of education were different between PTSD and HCs, although this factor is known not to be directly related with PTSD symptoms (Besser and Neria, 2009). Second, medication effects were not controlled in this study. Because all subjects were not in the first episode, some of them had undergone treatment with medication.

## 5. Conclusion

In this study, we demonstrated that a Riemannian geometry-based classifier could elevate the accuracy of classification of PTSD patients and HCs. Our findings also suggest that PTSD could be classified using resting-state EEG with significantly improved accuracy by adopting EEG source imaging and employing a novel type of classifiers such as

the FgMDM classifier. Further studies are required to generalize our findings by applying the Riemannian geometry-based classifier to the diagnosis of other psychiatric diseases and to enhance classification performance by employing new classification methods or source localization algorithms.

## Funding and disclosure

This work was supported by the National Research Foundation of Korea (NRF) grants (No. 2019R1A2C2086593 and NRF-2015M3C7A1028252) funded by the Korean government (MSIT). The authors declare no competing interests.

## Ethical statement

This study was reviewed and approved by the Institutional Review Board of Inje University, Ilsan Paik Hospital (IRB no. 2015-07-025) and conformed to the tenets of the Declaration of Helsinki.

## Author contributions

Y.W.K. analyzed the data and wrote the original draft. S.K. and M.S. analyzed the data. M.J.J. and H.J. collected the data. S.H.L. and C.H.I. conceptualized the study and reviewed the paper. All authors have approved the final version of the manuscript.

## Declaration of Competing Interest

The authors declare that they have no known competing financial interests or personal relationships that could have appeared to influence the work reported in this paper.

## References

- Ahn, M., Hong, J.H., Jun, S.C., 2012. Feasibility of approaches combining sensor and source features in brain-computer interface. *J. Neurosci. Methods* 204, 168–178. <https://doi.org/10.1016/j.jneumeth.2011.11.002>.
- American Psychiatric Association, 2013. *Diagnostic and Statistical Manual of Mental Disorders (Dsm-5)*. American Psychiatric Pub, Washington DC.
- Attias, J., Bleich, A., Gilat, S., 1996. Classification of veterans with post-traumatic stress disorder using visual brain evoked P3s to traumatic stimuli. *Br. J. Psychiatry* 168 (1), 110–115. <https://doi.org/10.1192/bjp.168.1.110>.
- Barachant, A., Congedo, M., 2014. A Plug&Play P300 BCI Using Information Geometry. (arXiv preprint. [arXiv:1409.0107](https://arxiv.org/abs/1409.0107)).
- Barachant, A., Bonnet, S., Congedo, M., Jutten, C., 2010. Riemannian Geometry Applied to BCI Classification. Paper presented at the International Conference on Latent Variable Analysis and Signal Separation. Springer, Berlin, Heidelberg, pp. 629–636.
- Barachant, A., Bonnet, S., Congedo, M., Jutten, C., 2011. Multiclass brain-computer interface classification by Riemannian geometry. *IEEE Trans. Biomed. Eng.* 59 (4), 920–928. <https://doi.org/10.1109/TBME.2011.2172210>.
- Barachant, A., Andreev, A., Congedo, M., 2013a. The Riemannian Potato: An Automatic and Adaptive Artifact Detection Method for Online Experiments Using Riemannian Geometry. *TOBI Workshop IV*, Sion, Switzerland, pp. 19–20.
- Barachant, A., Bonnet, S., Congedo, M., Jutten, C., 2013b. Classification of covariance matrices using a Riemannian-based kernel for BCI applications. *Neurocomputing* 112, 172–178. <https://doi.org/10.1016/j.neucom.2012.12.039>.
- Bareham, C.A., Manly, T., Pustovaya, O.V., Scott, S.K., Bekinschtein, T.A., 2015. Losing the left side of the world: rightward shift in human spatial attention with sleep onset. *Sci. Rep.* 4, 5092. <https://doi.org/10.1038/srep05092>.
- Besser, A., Neria, Y., 2009. PTSD symptoms, satisfaction with life, and prejudicial attitudes toward the adversary among Israeli civilians exposed to ongoing missile attacks. *J. Trauma. Stress.* 22 (4), 268–275. <https://doi.org/10.1002/jts.20420>.
- Blake, D.D., Weathers, F.W., Nagy, L.M., Kaloupek, D.G., Gusman, F.D., Charney, D.S., Keane, T.M., 1995. The development of a clinician-administered PTSD scale. *J. Trauma. Stress.* 8 (1), 75–90. <https://doi.org/10.1007/BF02105408>.
- Breiman, L., 2001. Random forests. *Mach. Learn.* 45 (1), 5–32. <https://doi.org/10.1023/A:1010933404324>.
- Casson, A.J., 2019. Wearable EEG and beyond. *Biomed. Eng. Lett.* 9 (1), 53–71. <https://doi.org/10.1007/s13534-018-00093-6>.
- Christova, P., James, L.M., Engdahl, B.E., Lewis, S.M., Georgopoulos, A.P., 2015. Diagnosis of posttraumatic stress disorder (PTSD) based on correlations of pre-whitened fMRI data: outcomes and areas involved. *Exp. Brain Res.* 233 (9), 2695–2705. <https://doi.org/10.1007/s00221-015-4339-0>.
- Coburn, K.L., Lauterbach, E.C., Boutros, N.N., Black, K.J., Arciniegas, D.B., Coffey, C.E., 2006. The value of quantitative electroencephalography in clinical psychiatry: a

- report by the committee on research of the American neuropsychiatric association. *J. Neuropsychiatr. Clin. Neurosci.* 18 (4), 460–500. <https://doi.org/10.1176/jnp.2006.18.4.460>.
- Congedo, M., Barachant, A., Bhatia, R., 2017. Riemannian geometry for EEG-based brain-computer interfaces; a primer and a review. *Brain Comp. Interfaces* 4 (3), 155–174. <https://doi.org/10.1080/2326263X.2017.1297192>.
- Congedo, M., Rodrigues, P., Jutten, C., 2019. The Riemannian minimum distance to means field classifier. In: 8th Graz Brain-Computer Interface Conference 2019. Austria, Graz. <https://doi.org/10.3217/978-3-85125-682-6-02>.
- Covey, T.J., Shucard, J.L., Violanti, J.M., Lee, J., Shucard, D.W., 2013. The effects of exposure to traumatic stressors on inhibitory control in police officers: a dense electrode Array study using a go/Nogo continuous performance task. *Int. J. Psychophysiol.* 87 (3), 363–375. <https://doi.org/10.1016/j.jpsycho.2013.03.009>.
- Cowdin, N., Kobayashi, I., Mellman, T.A., 2014. Theta frequency activity during rapid eye movement (REM) sleep is greater in people with resilience versus PTSD. *Exp. Brain Res.* 232 (5), 1479–1485. <https://doi.org/10.1007/s00221-014-3857-5>.
- Davoudi, A., Ghidary, S.S., Sadatnejad, K., 2017. Dimensionality reduction based on distance preservation to local mean for symmetric positive definite matrices and its application in brain-computer interfaces. *J. Neural Eng.* 14 (3), 036019. <https://doi.org/10.1088/1741-2552/a61bb>.
- Duda, R.O., Hart, P.E., Stork, D.G., 2012. *Pattern Classification*, 2nd edition. Wiley-Interscience New York, NY, USA.
- Ehlers, C.L., Hurst, S., Phillips, E., Gilder, D.A., Dixon, M., Gross, A., Lau, P., Yehuda, R., 2006. Electrophysiological responses to affective stimuli in American Indians experiencing trauma with and without PTSD. *Ann. N. Y. Acad. Sci.* 1071 (1), 125–136. <https://doi.org/10.1196/annals.1364.011>.
- Falconer, E.M., Felmingham, K.L., Allen, A., Clark, C.R., Mcfarlane, A.C., Williams, L.M., Bryant, R.A., 2008. Developing an integrated brain, behavior and biological response profile in Posttraumatic Stress Disorder (PTSD). *J. Integr. Neurosci.* 7 (3), 439–456. <https://doi.org/10.1142/S0219635208001873>.
- Fingelkurts, A.A., Fingelkurts, A.A., 2015. Altered structure of dynamic electroencephalogram oscillatory pattern in major depression. *Biol. Psychiatry* 77 (12), 1050–1060. <https://doi.org/10.1016/j.biopsych.2014.12.011>.
- Friedman, M.J., 2015. Overview of Posttraumatic Stress Disorder (PTSD). In: *Posttraumatic and Acute Stress Disorders*. Springer, Cham, pp. 1–8.
- Friedman, M.J., Resick, P.A., Bryant, R.A., Brewin, C.R., 2011. Considering PTSD for DSM-5. *Depress. Anxiety* 28 (9), 750–769.
- Galatzer-Levy, I.R., Karstoft, K.I., Statnikov, A., Shalev, A.Y., 2014. Quantitative forecasting of PTSD from early trauma responses: a machine learning application. *J. Psychiatr. Res.* 59, 68–76. <https://doi.org/10.1016/j.jpsychires.2014.08.017>.
- Gemein, L.A.W., Schirmmeister, R.T., Chrabaszcz, P., Wilson, D., Boedecker, J., Schulze-Bonhage, A., Hutter, F., Ball, T., 2020. Machine-Learning-Based Diagnostics of EEG Pathology. arXiv preprint arXiv:2002.05115.
- Goel, M.K., Chavarriga, R., Millán, J.D.R., 2011. Cortical current density vs. surface EEG for event-related potential-based brain-computer interface. In: Paper presented at the 2011 5th International IEEE/EMBS Conference on Neural Engineering, pp. 430–433.
- Gramfort, A., Papadopoulos, T., Olivi, E., Clerc, M., 2010. Openmeeeg: open-source software for quasistatic bioelectromagnetics. *Biomed. Eng. Online* 9 (1), 45. <https://doi.org/10.1186/1475-925X-9-45>.
- Han, C.H., Kim, Y.W., Kim, S.H., Nenadic, Z., Im, C.H., 2019. Electroencephalography-based endogenous brain-computer interface for online communication with a completely locked-in patient. *J. Neuroeng. Rehabil.* 16 (1), 18. <https://doi.org/10.1186/s12984-019-0493-0>.
- Harandi, M., Salzman, M., Hartley, R., 2017. Dimensionality reduction on SPD manifolds: the emergence of geometry-aware methods. *IEEE Trans. Pattern Anal. Mach. Intell.* 40 (1), 48–62. <https://doi.org/10.1109/TPAMI.2017.2655048>.
- Horev, I., Yger, F., Sugiyama, M., 2015. Geometry-Aware Principal Component Analysis for Symmetric Positive Definite Matrices. Paper presented at the ACML, pp. 1–16.
- Hsu, Y.L., Yang, Y.T., Wang, J.S., Hsu, C.Y., 2013. Automatic sleep stage recurrent neural classifier using energy features of EEG signals. *Neurocomputing* 104, 105–114. <https://doi.org/10.1016/j.neucom.2012.11.003>.
- Imperatori, C., Farina, B., Quintiliani, M.I., Onofri, A., Gattinara, P.C., Lepore, M., Gnani, V., Mazzucchi, E., Contardi, A., Della Marca, G., 2014. Aberrant EEG functional connectivity and EEG power spectra in resting state post-traumatic stress disorder: a sLORETA study. *Biol. Psychol.* 102, 10–17. <https://doi.org/10.1016/j.biopsycho.2014.07.011>.
- Kalunga, E.K., Chevallier, S., Barthélemy, Q., Djouani, K., Monacelli, E., Hamam, Y., 2016. Online SSVEP-based BCI using Riemannian geometry. *Neurocomputing* 191, 55–68. <https://doi.org/10.1016/j.neucom.2016.01.007>.
- Karl, A., Malta, L.S., Maercker, A., 2006. Meta-analytic review of event-related potential studies in post-traumatic stress disorder. *Biol. Psychol.* 71 (2), 123–147. <https://doi.org/10.1016/j.biopsycho.2005.03.004>.
- Kemp, A., Griffiths, K., Felmingham, K., Shankman, S.A., Drinkenburg, W., Arns, M., Clark, C.R., Bryant, R.A., 2010. Disorder specificity despite comorbidity: resting EEG alpha asymmetry in major depressive disorder and post-traumatic stress disorder. *Biol. Psychol.* 85 (2), 350–354. <https://doi.org/10.1016/j.biopsycho.2010.08.001>.
- Kessler, R.C., Berglund, P., Demler, O., Jin, R., Merikangas, K.R., Walters, E.E., 2005. Lifetime prevalence and age-of-onset distributions of DSM-IV disorders in the National Comorbidity Survey Replication. *Arch. Gen. Psychiatry* 62 (6), 593–602. <https://doi.org/10.1001/archpsyc.62.6.593>.
- Lee, S.H., Yoon, S., Kim, J.I., Jin, S.H., Chung, C.K., 2014. Functional connectivity of resting state EEG and symptom severity in patients with post-traumatic stress disorder. *Prog. Neuro-Psychopharmacol. Biol. Psychiatry* 51, 51–57. <https://doi.org/10.1016/j.pnpbp.2014.01.008>.
- Li, Y., Wong, K.M., deBruin, H., 2009. EEG Signal Classification Based on a Riemannian Distance Measure. Paper presented at the 2009 IEEE Toronto International Conference Science and Technology for Humanity (TIC-STH). pp. 268–273.
- Li, Y., Wong, K.M., de Bruin, H., 2012. Electroencephalogram signals classification for sleep-state decision—a Riemannian geometry approach. *IET Signal Process.* 6 (4), 288–299. <https://doi.org/10.1049/iet-spr.2011.0234>.
- Liu, F., Xie, B., Wang, Y., Guo, W., Fouché, J.P., Long, Z., Wang, W., Chen, H., Li, M., Duan, X., Zhang, J., Qiu, M., Chen, H., 2015. Characterization of post-traumatic stress disorder using resting-state fMRI with a multi-level parametric classification approach. *Brain Topogr.* 28 (2), 221–237. <https://doi.org/10.1007/s10548-014-0386-2>.
- Lobo, I., David, I.A., Figueira, I., Campagnoli, R.R., Volchan, E., Pereira, M.G., de Oliveira, L., 2014. Brain reactivity to unpleasant stimuli is associated with severity of posttraumatic stress symptoms. *Biol. Psychol.* 103, 233–241. <https://doi.org/10.1016/j.biopsycho.2014.09.002>.
- Lobo, I., Portugal, L.C., Figueira, I., Volchan, E., David, I., Pereira, M.G., de Oliveira, L., 2015. EEG correlates of the severity of posttraumatic stress symptoms: a systematic review of the dimensional PTSD literature. *J. Affect. Disord.* 183, 210–220. <https://doi.org/10.1016/j.jad.2015.05.015>.
- Metzger, L.J., Pitman, R.K., Miller, G.A., Paige, S.R., Orr, S.P., 2008. Intensity dependence of auditory P2 in monozygotic twins discordant for Vietnam combat: associations with posttraumatic stress disorder. *J. Rehabil. Res. Dev.* 45 (3), 437.
- Meyer, T., Quaedflieg, C.W., Weijland, K., Schruers, K., Merckelbach, H., Smeets, T., 2018. Frontal EEG asymmetry during symptom provocation predicts subjective responses to intrusions in survivors with and without PTSD. *Psychophysiology*. 55 (1), e12779. <https://doi.org/10.1111/psyp.12779>.
- Park, K.S., Choi, S.H., 2019. Smart technologies toward sleep monitoring at home. *Biomed. Eng. Lett.* 9 (1), 73–85. <https://doi.org/10.1007/s13534-018-0091-2>.
- Rabe, S., Beauducel, A., Zöllner, T., Maercker, A., Karl, A., 2006. Regional brain electrical activity in posttraumatic stress disorder after motor vehicle accident. *J. Abnorm. Psychol.* 115 (4), 687.
- Rodrigues, P., Bouchard, F., Congedo, M., Jutten, C., 2017. Dimensionality reduction for BCI classification using Riemannian geometry. In: Paper presented at the 7th Graz Brain-Computer Interface Conference (BCI 2017). Austria, Graz.
- Roy, R.N., Charbonnier, S., Bonnet, S., 2014. Detection of mental fatigue using an active BCI inspired signal processing chain. *IFAC Proc. Vol.* 47 (3), 2963–2968. <https://doi.org/10.3182/20140824-6-ZA-1003.00897>.
- Rozic, V., Vazquez-Reina, A., Crystal, M., Srivastava, A., Tan, V., Berka, C., 2014. Multi-modal prediction of PTSD and stress indicators. In: Paper presented at the 2014 IEEE International Conference on Acoustics, Speech and Signal Processing (ICASSP), pp. 3636–3640.
- Rubinov, M., Sporns, O., 2010. Complex network measures of brain connectivity: uses and interpretations. *Neuroimage* 52 (3), 1059–1069. <https://doi.org/10.1016/j.neuroimage.2009.10.003>.
- Ruhnau, B., 2000. Eigenvector-centrality—a node-centrality? *Soc. Networks* 22 (4), 357–365. [https://doi.org/10.1016/S0378-8733\(00\)00031-9](https://doi.org/10.1016/S0378-8733(00)00031-9).
- Rutkowski, T.M., Zhao, Q., Abe, M.S., Otake, M., 2018. AI Neurotechnology for Aging Societies—Task-load and Dementia EEG Digital Biomarker Development Using Information Geometry Machine Learning Methods. arXiv preprint arXiv:1811.12642.
- Sadatnejad, K., Rahmati, M., Rostami, R., Kazemi, R., Ghidary, S.S., Müller, A., Alimardani, F., 2019. EEG representation using multi-instance framework on the manifold of symmetric positive definite matrices. *J. Neural Eng.* 16 (3), 036016. <https://doi.org/10.1088/1741-2552/ab0dad>.
- Scheeringa, M.S., Zeanah, C.H., Drell, M.J., Larrieu, J.A., 1995. Two approaches to the diagnosis of posttraumatic stress disorder in infancy and early childhood. *J. Am. Acad. Child Adolesc. Psychiatry* 34 (2), 191–200. <https://doi.org/10.1097/00004583-199502000-00014>.
- Scholkopf, B., Sung, K.K., Burges, C.J., Girosi, F., Niyogi, P., Poggio, T., Vapnik, V., 1997. Comparing support vector machines with Gaussian kernels to radial basis function classifiers. *IEEE Trans. Signal Process.* 45, 2758–2765. <https://doi.org/10.1109/78.650102>.
- Semlitsch, H.V., Anderer, P., Schuster, P., Presslich, O., 1986. A solution for reliable and valid reduction of ocular artifacts, applied to the P300 ERP. *Psychophysiology* 23 (6), 695–703. <https://doi.org/10.1111/j.1469-8986.1986.tb00696.x>.
- Sheerin, C.M., Franke, L.M., Aggen, S.H., Amstadter, A.B., Walker, W.C., 2018. Evaluating the contribution of EEG power profiles to characterize and discriminate posttraumatic stress symptom factors in a combat-exposed population. *Clin EEG Neurosci.* 49 (6), 379–387. <https://doi.org/10.1177/2155005918767583>.
- Shim, M., Hwang, H.J., Kim, D.W., Lee, S.H., Im, C.H., 2016. Machine-learning-based diagnosis of schizophrenia using combined sensor-level and source-level EEG features. *Schizophr. Res.* 176 (2–3), 314–319. <https://doi.org/10.1016/j.schres.2016.05.007>.
- Strijkstra, A.M., Beersma, D.G., Drayer, B., Halbesma, N., Daan, S., 2003. Subjective sleepiness correlates negatively with global alpha (8–12 Hz) and positively with central frontal theta (4–8 Hz) frequencies in the human resting awake electroencephalogram. *Neurosci. Lett.* 340 (1), 17–20. [https://doi.org/10.1016/S0304-3940\(03\)00033-8](https://doi.org/10.1016/S0304-3940(03)00033-8).
- Šušmáková, K., Krakovská, A., 2007. Classification of waking, sleep onset and deep sleep by single measures. *Sci. Rev.* 7, 34–38.
- Tadel, F., Baillet, S., Mosher, J.C., Pantazis, D., Leahy, R.M., 2011. Brainstorm: a user-friendly application for MEG/EEG analysis. *Comput. Intell. Neurosci.* 2011, 8. <https://doi.org/10.1155/2011/879716>.
- Todder, D., Levine, J., Abujumah, A., Mater, M., Cohen, H., Kaplan, Z., 2012. The quantitative electroencephalogram and the low-resolution electrical tomographic analysis in posttraumatic stress disorder. *Clin. EEG Neurosci.* 43 (1), 48–53. <https://doi.org/10.1177/1550059411428716>.
- Wahbeh, H., Oken, B.S., 2013. Peak high-frequency HRV and peak alpha frequency higher in PTSD. *Appl. Psychophysiol. Biofeedback* 38 (1), 57–69. <https://doi.org/10.1007/>

s10484-012-9208-z.

Weathers, F.W., Litz, B.T., Herman, D.S., Huska, J.A., Keane, T.M., 1993. The PTSD checklist (PCL): reliability, validity, and diagnostic utility. In: Paper presented at the Annual Convention of the International Society For Traumatic Stress Studies, San Antonio, TX. 462.

Woodward, S.H., Murburg, M.M., Bliwise, D.L., 2000. PTSD-related hyperarousal assessed during sleep. *Physiol. Behav.* 70 (1–2), 197–203. <https://doi.org/10.1016/S0031->

9384(00)00271-7.

Yuan, S., Zhou, W., Wu, Q., Zhang, Y., 2016. Epileptic seizure detection with log-euclidean gaussian kernel-based sparse representation. *Int. J. Neural Syst.* 26 (3), 1650011. <https://doi.org/10.1142/S0129065716500118>.

Zhuang, X., Rozgić, V., Crystal, M., Marx, B.P., 2013. Improving Speech-Based PTSD Detection Via Multi-View Learning. *IEEE Spoken Language Technology Workshop (SLT)*, South Lake Tahoe, NV, pp. 260–265.